Improvement of aerosol optical depth retrieval from MODIS spectral reflectance over the global ocean using new aerosol models archived from AERONET inversion data and tri-axial ellipsoidal dust database data

J. Lee[1,2,3], J. Kim[1,4] *, P. Yang[5], and N. C. Hsu[3]

[1]{Institute of Earth, Astronomy, and Atmosphere, Brain Korea 21 Program, Department of Atmospheric Sciences, Yonsei University, Seoul, Republic of Korea}

Now at [2]{Earth System Science Interdisciplinary Center, University of Maryland College Park, College Park, MD, USA}

[3]{NASA Goddard Space Flight Center, Greenbelt, MD, USA}

[4]{Joint Institute for Regional Earth System Science and Engineering, University of California Los Angeles, Los Angeles, CA, USA}

[5]{Department of Atmospheric Sciences, Texas A&M University, College Station, TX, USA}

Correspondence to: Jhoon Kim (jkim2@yonsei.ac.kr)

Abstract

New over-ocean aerosol models are developed by integrating the inversion data from the Aerosol Robotic Network (AERONET) sun/sky radiometers with a database for the optical properties of tri-axial ellipsoids. The new aerosol models allow more accurate retrieval of aerosol optical depth (AOD) from the Moderate Resolution Imaging Spectroradiometer (MODIS) in the case of high AOD (AOD > 0.3). The aerosol models are categorized by using the fine-mode fraction (FMF) at 550 nm and the single-scattering albedo (SSA) at 440 nm from the AERONET inversion data to include a variety of aerosol types found around the globe. For each aerosol model, the changes in the aerosol optical properties (AOP) as functions of AOD are considered to better represent aerosol characteristics. Comparisons of AODs between AERONET and MODIS for the period from 2003 to 2010 show that the use of the new aerosol models enhances the AOD accuracy with a Pearson coefficient of 0.93 and

a regression slope of 0.99 compared to 0.92 and 0.85 calculated using the MODIS Collection 5 data. Moreover, the percentage of data within an expected error of $\pm(0.03 + 0.05 \times AOD)$ is increased from 62% to 64% for overall data and from 39% to 51% for AOD > 0.3. Errors in the retrieved AOD are further characterized with respect to the Ångström exponent (AE), scattering angle (Θ), SSA, and air mass factor (AMF). Due to more realistic AOP assumptions, the new algorithm generally reduces systematic errors in retrieved AODs compared with the current operational algorithm. In particular, the underestimation of fine-dominated AOD and the scattering angle dependence of dust-dominated AOD are significantly mitigated as results of the new algorithm's improved treatment of aerosol size distribution and dust particle nonsphericity.

1   Introduction

Aerosols exert a significant impact on climate change and air quality. The small airborne particles regulate the radiation budget through both direct and indirect effects (IPCC, 2007), specifically, by scattering and absorbing radiation and by modifying cloud microphysics. Aerosols are known to affect human health by causing and worsening respiratory illnesses (Pope and Dockery, 2006). Because the spatio-temporal distribution of aerosols is highly variable, satellite observations have been extensively utilized to quantify aerosol optical properties (AOP) over wide areas and with fine spatio-temporal resolution.

Traditional 5-channel meteorological imagers, including single visible-band instruments aboard geostationary satellites, are used to continuously monitor aerosol optical depth (AOD), but have a limited ability to retrieve other parameters (Knapp et al., 2002; Wang et al., 2003; Kim et al., 2008). In contrast, multi-spectral instruments on board low Earth orbit (LEO) satellites, such as the Advanced Very High Resolution Radiometer (AVHRR), Sea-viewing Wide Field-of-view Sensor (SeaWiFS), and Moderate Resolution Imaging Spectroradiometer (MODIS), can retrieve aerosol size information and absorptivity (Higurashi and Nakajima, 1999; Mishchenko et al., 1999; Higurashi and Nakajima, 2002; Hsu et al., 2004; Remer et al., 2005; Hsu et al., 2006; Kim et al., 2007; Levy et al., 2007b). The Geostationary Ocean Color Imager (GOCI), which observes spectral radiances centered at 412, 443, 490, 555, 660, 680, 745, and 865 nm from a geostationary orbit, has been used for hourly monitoring of AOD and to retrieve the fine-mode fraction (FMF) and aerosol types over East Asia (Lee et al., 2010b).

With their wide spatial and spectral coverage, the observations made by the MODIS instruments aboard the Terra and Aqua satellites provide an unprecedented opportunity to infer AOP. MODIS has 36 spectral bands ranging from 0.41 to 15 μm with three different spatial resolutions (250 m, 500 m, 1 km) and with 2300 km-wide swath coverage. Since the launches of MODIS in 1999 for Terra and 2002 for Aqua, numerous efforts have been made to retrieve, evaluate, and improve the aerosol products obtained. The original operational algorithms for dark vegetated areas (Kaufman et al., 1997) and oceans (Tanré et al., 1997) are two very important additions. The MODIS algorithms have been frequently updated to improve the quality of retrieved data by modifying cloud-masking processes, aerosol models, and the surface reflectance database (Remer et al., 2005; Levy et al., 2007a; Levy et al., 2007b). Hsu et al. (2006) developed Deep-Blue algorithm, which is applicable to bright land surfaces including desert areas, to facilitate monitoring of dust aerosols over source regions. Consequently, the current MODIS operational algorithms provide the columnar aerosol amount (AOD) and size information (FMF, Ångström exponent [AE]) for full coverage of the Earth except for cloud- and snow-covered areas. In addition, the Deep-Blue algorithm also has the ability to retrieve the single-scattering albedo (SSA) of dust aerosols.

MODIS aerosol products have been validated extensively to evaluate data quality. Preliminary comparisons of AOD from Terra-MODIS with that observed from Aerosol Robotic Network (AERONET) Sun/sky radiometers (Holben et al., 1998) showed that the AOD at 660 nm over the ocean differed by only 2% on average, with negligible offset (Remer et al., 2002), while the Terra-MODIS AOD over land was underestimated by about 14% except for coastal areas (Chu et al., 2002). However, the comparison results for land varied significantly with location, partially due to different surface conditions and aerosol sources. On the contrary, a validation by Remer et al. (2008) showed an almost perfect regression slope for the AOD at 550 nm over land as calculated by AERONET and MODIS, but an underestimation of AOD over the ocean from Aqua-MODIS, in particular for high AODs. It should be noted that the land algorithm has been modified substantially to resolve better aerosol models and surface reflectance (Levy et al., 2007a; Levy et al., 2007b), whereas no substantial update has been made to the original ocean algorithm (Remer et al., 2005, 2006). Therefore, the significant improvement in the regression slope over land is likely attributed to improved aerosol models to some extent, because the slope largely depends on data in the high AOD regime where the aerosol signal dominates the surface signal.

1   In this paper, new aerosol models are introduced by integrating AERONET inversion data

2   (Dubovik and King, 2000; Dubovik et al., 2006) with single-scattering property data from a

3   tri-axial ellipsoidal dust database (Meng et al., 2010). The AOPs of each aerosol model are

4   used to calculate a lookup table (LUT) for spectral reflectances from MODIS. By using the

5   LUT, retrieval and validation of AODs are performed over the global ocean using Aqua-

6   MODIS data to improve the underestimation of AOD reported by Remer et al. (2008). The

7   validation results are compared with those from the current operational algorithm to further

8   characterize the effects of the new aerosol models.

9

10   2   MODIS ocean algorithms

11   Remer et al. (2005, 2006) described the current MODIS Collection 5 operational over-ocean

12   algorithm (hereafter, C005 algorithm) in detail. The algorithm retrieves spectral AOD and

13   FMF using spectral reflectances centered at 555, 650, 860, 1240, 1630, and 2120 nm by

14   comparing observed and pre-calculated reflectances. To this end, sophisticated forward

15   radiative transfer simulations of the the reflectances (i.e. LUT) need to be performed for

16   various aerosol models, surface reflectances, and sun/satellite geometries. Because the top-of-

17   atmosphere (TOA) reflectance consists of signals from both the surface and atmosphere, the

18   algorithm specifies surface reflectance in terms of the Fresnel reflection accounting for sea-

19   surface roughness with a wind speed of 6 m/s and zero water-leaving radiance except at 550

20   nm where a water-leaving radiance of 0.005 is assumed. The atmospheric contribution,

21   aerosols in particular, is calculated using four fine-mode and five coarse-mode aerosols. Then,

22   both spectral AOD and FMF (550 nm), a ratio of fine-mode AOD to total AOD, are

23   simultaneously retrieved by minimizing the error between the observed and calculated

24   reflectances for each of the 20 combinations from the fine- and coarse-mode aerosol models

25   with the fixed AOD retrieved from 860 nm.

26   A schematic flowchart of the C005 algorithm and a test algorithm to evaluate the effects of

27   the new aerosol models introduced in this paper is provided in Figure 1. The test algorithm is

28   designed to use the same spectral reflectances as the C005 algorithm in order to constrain

29   other effects that can arise from different pre-processing of the data. We used the

30   "Mean_Reflectance_Ocean" product in the "MYD04" files, which provides cloud- and

31   sediment-masked mean reflectance in 20 × 20 pixels of 500 m pixel-resolution data at seven

32   wavelengths centered at 470, 555, 650, 860, 1240, 1630, and 2120 nm. The product is the

same as that used in the C005 algorithm. The major difference between the two algorithms is the aerosol model, and minor change is made to the inversion procedure. The test algorithm first retrieves AOD at 550 nm using every wavelength and aerosol model, and then selects the aerosol model that minimizes the standard deviation of the seven different AODs at 500 nm retrieved from each wavelength. The final AOD is chosen according to the selected aerosol model. By doing so, each wavelength contributes equally to selecting the aerosol model, whereas 860 nm band has strong weighting in the C005 algorithm due to the calculation of spectral fitting error between observed- and simulated-reflectances with a perfect match at 860 nm in selecting aerosol model. In addition, for the low AOD case (AOD $\leq$ 0.15), the test algorithm uses only longer wavelengths (650, 860, 1240, 1630, 2120 nm), at which the water-body absorption is strong, and thereby reduces errors from the assumed surface reflectance, whereas the algorithm uses all the seven bands for AOD > 0.15. As a result, the algorithm retrieves AOD and aerosol model, i.e., FMF and SSA, simultaneously. Note that no combination between aerosol models is assumed in the test algorithm in contrast to the operational algorithm.

3   New aerosol models

Use of a radiative transfer model (RTM) to simulate satellite-observed TOA reflectance requires aerosol characteristics such as spectral refractive indices, size distribution, and nonsphericity to describe nonspherical particles. Otherwise, the spectral AOD, SSA, and phase function, which are derived from the aforementioned aerosol properties, are required. Thus, long-term AERONET inversion data that provides the AOP for the globe can be used to simulate the satellite signal for various aerosol types. It should be noted that the AERONET observes ambient-columnar properties similar to those obtained from satellite observations, while in-situ measurements provide near-ground properties. Moreover, the AERONET-retrieved AOP represent the radiation field well for the wide scattering angle range, because the inversion data are retrieved to match the calculated radiation field with the observed sky radiances from the combined principal/almucantar planes (Dubovik and King, 2000; Dubovik et al., 2006). The inversion data provide AOP at 440, 675, 870, and 1020 nm, but for MODIS observations, the tri-axial ellipsoidal dust database introduced in the work of Meng et al. (2010) is required to expand the wavelength range up to 2120 nm.

5

3.1 AERONET inversion data

The quality-assured, "Level 2 Inversion All Points" data are used to derive aerosol models over the ocean for the test algorithm. To this end, data needs to be collected from specific AERONET stations chosen by distance from the ocean. The distance from the ocean is calculated by using geo-location information for each AERONET site and a high-resolution digital elevation model (DEM). The criterion for selecting the coastal stations was the distance within 7 km from the ocean. Figure 2 shows the 81 selected stations and the number of inversion data available to date. Although large portions of the data are from the U.S. and Europe, where anthropogenic aerosols are dominant, the AERONET data in the downwind of North Africa are expected to provide AOPs of transported dust and biomass-burning aerosols. The data also cover dust aerosols transported from the Arabian Desert, both anthropogenic and dust aerosols over East Asia, and marine aerosols over the remote ocean. However, only one site is located downwind of Southern Africa and a lack of data may lead to uncertainties in the AOP of biomass-burning aerosols from the area.

Aerosol models incorporated into satellite algorithms should account for the various aerosol types that exist and cause differences in the radiation field in order for the appropriate aerosol models to be selected from the observed radiation field. Therefore, use of size and absorptivity to classify aerosol types is the most reasonable method for remote sensing applications, because the two parameters directly affect the radiation field (Dubovik et al., 2002; Levy et al., 2007a; Mielonen et al., 2009; Lee et al., 2010a). While MODIS operational algorithms adopt fine- and coarse-mode aerosols separately and combine their signals during retrieval, the test algorithm adopts independent mixture-type models by classifying aerosol types from the AERONET explicitly with respect to the FMF (550 nm) and the SSA (440 nm) (Lee et al., 2010b).

Figure 3 shows the number of aerosol events with specific FMF and SSA values observed by AERONET throughout the globe and in coastal areas. The global data infers that aerosols from different locations have a wide range of FMF and SSA values, indicating the presence of various aerosol types with small to large particles and both absorbing and non-absorbing. For FMF less than 0.4 (coarse-mode dominance), the SSA generally ranges from 0.85 to 0.95, indicating absorption of blue-wavelengths by the coarse particle-dominated aerosols. Because Level 2 inversion data provides SSA for AOD (440 nm) > 0.4, the coarse particle-dominated aerosols mainly represent dust events. Note that sea salt, a non-absorbing coarse-mode aerosol,

generally occurs with low AOD values. For fine particle-dominated aerosols (FMF > 0.6), the range of values for SSA is wider than that for coarse particle-dominated aerosols. The high SSA values correspond to non-absorbing anthropogenic aerosols such as sulfates and nitrates; whereas, the low SSA values imply the presence of black carbon (BC) (Hess et al., 1998; Wang and Martin, 2007). The major difference between global and coastal data is highlighted by the lack of data in the extremely low SSA regime. The high relative humidity (RH) in coastal areas, the aging of BC during transport, and the few AERONET stations in downwind of biomass-burning aerosols may cause the result. Both high RH and BC aging are known to increase SSA (Wang and Martin, 2007).

Based on the representation of aerosol types classified using FMF and SSA (Lee et al., 2010a), aerosol models are created by quantized square-bins over the FMF and SSA domains. Binning intervals of 0.1 and 0.05 are used for FMF and SSA, respectively. Each aerosol model is further categorized as a function of AOD by averaging AOP between fore- and aft-medians of each AOD nodal point. If no data exist for a higher AOD bin, the AOP of the previous bin is used. Consequently, the spectral AOD, SSA, and phase function are averaged over the three-dimensional domains of FMF, SSA, and AOD to be used as input data for the LUT calculations. Prior to the averaging, spectral AOD is normalized by itself at 550 nm and multiplied by each AOD nodal point. This method, however, has limited application to low AOD data, because SSA is retrieved only for AOD (440 nm) > 0.4. As an alternative, the SSA is assumed to be 0.99, regardless of the wavelength, by considering the sea salt dominance in the low AOD regime over the ocean, while the other parameters (spectral AOD, phase function) are compiled from AERONET inversion data. As a result, a total of 23 aerosol models are created with the number of data points constrained to be greater than 10 for each aerosol model. The aerosol models cover FMF ranging from 0.2 to 1.0 for 0.85 < SSA < 0.95 (16 types) and from 0.3 to 1.0 for SSA > 0.95 (7 types). Dimensions of the LUT are summarized in Table 1.

3.2 Tri-axial ellipsoidal dust database

The AERONET inversion data provide AOP for wavelengths ranging from 440 nm to 1020 nm, while the MODIS observations cover the wavelengths from 470 nm to 2120 nm. To expand the wavelength range of AERONET AOP, data from the tri-axial ellipsoidal dust database (Meng et al., 2010) are used in this study. The database containing the single-scattering properties of individual tri-axial ellipsoidal particles is computed using the

Lorentz-Mie code (Bohren and Huffman, 1983), the T-matrix code (Mishchenko and Travis, 1998), the Amsterdam discrete dipole approximation (DDA) code (Yurkin and Hoekstra, 2009), and the improved geometric optics method (IGOM) code (Yang and Liou, 1996; Yang et al., 2007; Bi et al., 2009). Because tri-axial ellipsoidal shapes include spheres and ellipsoids with a number of aspect ratios, the application of the database can be expanded to non-dust aerosols. The database provides extinction efficiency, SSA, phase matrix, etc., for various refractive indices, size parameters, and aspect ratios, thus the proxy of the AERONET AOP (spectral AOD, SSA, and phase function) can be extracted when given the spectral refractive indices, size distribution, aspect ratios, and nonsphericity. Among the required parameters, only refractive indices are functions of wavelength. As a result, the refractive indices used in the C005 algorithm (Remer et al., 2005, 2006), are used for the longer wavelengths ($\lambda \geq 1240$ nm) with the given size distribution and nonsphericity from the AERONET data. The refractive indices of "water soluble" and "water soluble with humidity" from the C005 aerosol models are used for fine-mode ($0.85 < \text{SSA} < 0.95$ and $\text{SSA} > 0.95$, respectively), and the refractive indices of "dust-like type" and "wet sea salt type" are used for coarse-mode ($\text{AOD} > 0.1$ and $\text{AOD} = 0.1$, respectively). Although the refractive indices of the MODIS aerosol models are not completely consistent with those of the new aerosol models, the low sensitivity at longer wavelengths ($\lambda \geq 1240$ nm) to the fine-mode aerosols and the relatively well-known absorption properties of dust (almost non-absorbing) are expected to result in smaller errors compared to excluding the longer wavelengths in the retrieval algorithm. With regard to nonsphericity and aspect ratios, mean "% sphericity" from the AERONET data and fixed spheroid mixture distribution are used as described in Dubovik et al. (2006). The dataset compiled by combining the AERONET inversion data and tri-axial ellipsoidal dust database data is used as input data into RTM calculations. The optical properties of the 23 aerosol models are summarized in Table 2. To calculate the LUT, a discrete ordinate radiative transfer (DISORT) code implemented into the libRadtran software package (Mayer and Kylling, 2005) is used. Due to the advantage of direct inputting the phase function into the libRadtran package, nonsphericity, which mainly affects phase function, can be readily handled with the software. However, the polarization effect is not included the same as in the C005 algorithm.

4   Sensitivity study

The possible differences in retrieved AOD between the C005 algorithm and test algorithm and the inversion accuracy are analysed before applying the developed algorithm to actual TOA reflectance data. Figure 4 shows the difference in the calculated TOA reflectance values between the C005 aerosol models and the new aerosol models for different AOD values at 860 nm, the reference wavelength used in selecting aerosol models from the C005 algorithm. The other wavelengths show similar tendencies. The corresponding C005 aerosol models to the new aerosol models are created by combining the F2 ("water soluble") and C8 ("dust-like type") aerosol models in Remer et al. (2006) for SSA < 0.95 and the F4 ("water solublt with humidity") and C8 for SSA > 0.95 by using FMF values from the new aerosol models. The results generally show that the C005 aerosol models overestimate the TOA reflectance, i.e., underestimation of AOD with a given TOA reflectance, compared to the new aerosol models, and the overestimation tends to increase with AOD and absorptivity. The increasing overestimation with AOD is mainly due to the increasing particle size with AOD from the new aerosol models. Increasing particle size results in decreasing TOA reflectance due to a decrease in the back-scattering fraction of reflected radiation. Only a few underestimations are found in dust-dominated models (H2, H3, H4, M2) and in non-absorbing models (N1 through N7) in the side-scattering case for low AOD. On the other hand, consistent overestimation is present in the back-scattering direction, indicating difference in phase function between spherical and nonspherical particles. The phase function of spherical particle has lower values at side-scattering angles and higher values at back-scattering angles compared to their nonspherical counterparts. The underestimation from the C005 aerosol model for non-absorbing fine-mode (N5 through N7) for low AOD is partially due to larger particle size of the F4 aerosol model compared with the fine-mode of the new aerosol model counterparts for low AOD. As a result, general underestimation of AOD is expected from the C005 algorithm compared with the test algorithm, and this may have caused the underestimation of high AOD in the validation results represented in Remer et al. (2008).

The inversion accuracy of the test algorithm with the new aerosol models is analysed by retrieving AOP using calculated TOA reflectances as a proxy for observation data. The test is performed for the whole LUT dimensions shown in Table 1 (total 283,176 data points), and, consequently, the AOD, FMF, and SSA are retrieved using both original TOA reflectance data and synthesized data including maximum random error of 3%. Figure 5 compares the

9

1 input data and retrieved results. The data points with regard to various geometries and the

2 other variables, except the target variable, are averaged at each nodal point and shown with

3 one-standard deviation intervals. The comparison results show that the inversion algorithm

4 completely reproduces the input variables if no errors are included in the TOA reflectance,

5 while small errors arise if maximum 3% errors are added to the reflectance data. However, the

6 mean values are almost perfect regardless of the variables, and one-standard deviation of the

7 AOD errors are well within the MODIS over-ocean expected error ($\pm[0.03 + 0.05 \times AOD]$).

8 Note that the 23 aerosol models appear to produce chracteristic spectral reflectance features,

9 to be selected by inversion procedure without producing significant interference one another.

10

5   Results and evaluation

12 The effects of the new aerosol models on AOD retrieval are evaluated by comparing the

13 AODs from AERONET and MODIS data retrieved by the C005 and the test algorithm. Eight

14 years of spectral reflectance data (2003 – 2010) observed from Aqua-MODIS are collected

15 and processed to retrieve AOD using the new aerosol models. The AOD data from the C005

16 algorithm are also processed to compare with the AERONET observations, thereby allowing

17 validation results from both algorithms to be compared. In this study, the

18 "Effective_Optical_Depth_Average_Ocean" data in the MYD04 files are used for the C005

19 algorithm. Overall statistical scores and systematic errors are compared to characterize

20 various error sources.

5.1   Overall evaluation

22 Figure 6 compares AODs between AERONET and MODIS over the global ocean from 2003

23 to 2010. Three different results retrieved from the C005 algorithm and test algorithm using

24 two different inversion procedures described in Section 2 are shown to investigate effects of

25 new aerosol models and inversion methods on AOD retrieval accuracy. For this comparison,

26 collocation was made within ±30 minutes in time and 25 km in space similar to the method

27 proposed by Ichoku et al. (2002). However, we sampled satellite pixels by calculating actual

28 distances between each AERONET location and the MODIS pixels for both test and

29 operational datasets, while Ichoku et al. (2002) selected 5×5 MODIS pixels with an

30 AERONET station located in the middle of the grid regardless of viewing angle. A criterion

31 are applied for the number of data points, which requires at least 5 and 2 data points for

MODIS and AERONET, respectively. Because the test algorithm tended to retrieve more data than the C005 algorithm due to the absence of a quality-control procedure used in C005 algorithm, only overlapping data retrieved by both algorithms were used for quantitative comparisons.

The validation results show that the AOD data from the C005 algorithm are highly correlated with the observations, but, on average, tend to be underestimated, with a Pearson coefficient of 0.92 and a regression slope of 0.85. The negative bias of the slope is caused by overestimation in the low AOD regime (AOD < 0.2) and underestimation in the high AOD regime (AOD > 0.3). Meanwhile, the new aerosol models improve the slope significantly (0.99 − 1.02) with a comparable correlation coefficient (0.93) regardless of the inversion methods. Only small differences are observed between the two results, showing a slight increase in statistics for the new inversion compared with the C005 inversion. However, the new inversion may not guarantee improved results for the C005 algorithm because of differences in the LUT. Since the difference is negligible between the two methods, only results from the new inversion will be shown for further analyses. From the statistics summarized in Table 3 and Table 4, the aerosol models clearly improve almost all the statistics analysed in this study. The slope and the percentage of data within an expected error improved from 62% to 64% overall and from 39% to 51% for AOD > 0.3. These improvements are particularly noticeable for the high AOD regime at which the aerosol signal dominates the other contributions such as Rayleigh scattering and surface reflectance. The major reason for the improvement in AOD retrieval is the consideration of absorbing fine-mode aerosols and changing the size distribution as a function of AOD. Both factors are expected to increase AOD for a given TOA reflectance (Levy et al., 2007b; Wang and Martin, 2007; Jethva et al., 2010). Note that the current MODIS algorithm adopts four different water-soluble aerosol models with fixed radii insensitive to AOD for the fine-mode cluster.

5.2 Error characteristics

Errors in AOD can arise from various sources including incorrect assumptions about surface reflectance and aerosol type, status of sensor calibration, observation geometry, etc. In addition, specific observation environments can bias results. Levy et al. (2010) evaluated the C005 over-land AOD data with regard to AE, cloud fraction, surface type characteristics, and observation geometry to characterize systematic error sources. Thus, the analyses to be

1 presented here together with the work of Levy et al. (2010) represent a complete evaluation of

2 the MODIS data retrieved over land and ocean.

3 Figure 7 shows the AE dependence of the retrieval errors for the C005 and the test algorithms.

4 The data were sorted into 20 and 10 equal-number-of-data bins for the overall data and AOD

5 > 0.3, respectively. As shown in the result, the C005 algorithm tends to overestimate coarse-

6 dominated AOD (AE < 0.8) and underestimate fine-dominated AOD (AE > 1.6). The

7 underestimation of fine-dominated AOD worsens for high AOD cases, suggesting that the

8 underestimation of high AOD from C005 algorithm shown in Figure 6 is mainly caused by

9 fine-dominated cases, while reliable retrievals are performed for dust aerosols. The retrieved

10 AODs are less stable (stability inferred by the magnitude of one standard deviation interval)

11 for fine-dominated AOD than coarse-dominated AOD, while stable retrieval is observed for

12 0.75 < AE < 1.4 partially due to the relatively low AOD. In the case of AOD > 0.3, although

13 there are systematic underestimations, the algorithm shows small mean biases (MBs) for

14 strong dust events (AE < 0.4) with higher stability than fine-dominated case (AE > 1.4).

15 The AE dependence of MB for the test algorithm is reduced overall compared with the C005

16 algorithm, but the test algorithm still has a tendency to overestimate coarse-dominated AOD

17 and to underestimate fine-dominated AOD. The AE dependence is reduced further for AOD >

18 0.3, but the AODs are distinctly overestimated for coarse-dominated case (AE < 0.3).

19 However, the standard deviation of the retrieval errors is slightly lower than that of the C005

20 algorithm for the coarse-dominated regime, while the standard deviation is similar between

21 the two algorithms for the fine-dominated regime (AE > 1.3). As a result, the new aerosol

22 models can be inferred to mitigate systematic errors (i.e., MB) compared with the C005

23 algorithm except for severe dust events (AOD > 0.3, AE < 0.3).

24 Figure 8 shows the scattering angle dependence of the retrieval errors. For overall case of the

25 C005 algorithm, the MB decreases gradually with increasing scattering angle and mean AOD.

26 The decrease is a result of combined effects of the systematic overestimation of low AOD

27 cases (AOD < 0.2) and the underestimation of fine-dominated AOD with increasing AOD. In

28 contrast, the scattering angle dependence of the MB is much lower in the test algorithm,

29 indicating improved retrieval accuracy. Only two distinct positive peaks are present for $140^{o} <$

30 $\Theta < 165^{o}$. For AOD > 0.3, the C005 algorithm shows systematic underestimation, while the

31 test algorithm shows positive MB for $\Theta > 140^{o}$ and negative MB for $\Theta < 140^{o}$. The

32 underestimation in the C005 algorithm tends to worsen with increasing scattering angle,

partially due to increasing AOD, while high AOD seems to correspond to low MB in the test algorithm.

For a more detailed explanation on the scattering angle dependence of the retrieval errors, additional comparisons for aerosol type information are shown in Figure 9. Note that neglecting the nonsphericity of dust particles results in underestimation of AOD in the back-scattering direction and overestimation in the side-scattering direction due to the difference in scattering phase function between spherical and nonspherical particles. For a dust-dominated case (AE < 0.8), the data provided by the C005 algorithm shows an imprint of the difference in phase functions between spherical and nonspherical particles, while the new aerosol models significantly reduce the scattering angle dependence. The new aerosol models, however, systematically overestimate the AOD regardless of the scattering angle. Consequently, the small MB of the C005 algorithm for coarse-dominated AOD, represented in Figure 7, can be explained by cancellation of the positive and negative errors, while the test algorithm systematically overestimates AOD. For anthropogenic aerosols (AE > 1.2), neither algorithm shows distinct features related to differences in the phase function, while the systematic underestimation of the C005 algorithm in the back-scattering direction is significantly reduced by the test algorithm.

The retrieval results are further categorized with respect to the SSA in order to understand the impact of aerosol absorption on retrieval accuracy. Figure 10 shows the MB of the retrieved AODs for SSA. The AE constraint is also applied to separate fine-dominated and coarse-dominated cases. The daily mean SSA values from AERONET are used in this investigation since insufficient data points are gathered if a time constraint is applied. Note that AERONET Level 2 SSA values are retrieved for AOD (440 nm) > 0.4. Thus, fine-dominated (AE > 1.2) and coarse-dominated cases (AE < 0.8) represent anthropogenic and dust events, respectively. For coarse-dominated case, no distinct dependence on SSA is observed for either dataset, but systematic overestimation of dust AOD from the test algorithm is highlighted. However, smaller standard deviations from the test algorithm indicate systematic error, while C005 algorithm shows somewhat larger dispersions. On the other hand, relatively strong absorptivity dependence is observed in the C005 algorithm for fine-dominated case, showing increasing underestimation tendency with SSA. In fact, the result is confusing because no highly absorbing aerosol model is included in the C005 algorithm and underestimation of absorptivity normally results in underestimation of AOD. However, the complexity of error

sources can produce the anomaly. As found in this study, both absorptivity and particle size assumed in the retrieval algorithm can cause errors in the retrieved AOD. In addition, errors in the retrieved FMF can result in additional error in the AOD. The results from the test algorithm show relatively accurate AOD retrieval with mitigated SSA dependence.

The sensitivity of TOA reflectance to AOD increases with air mass because of the increasing optical path. Thus, the air mass factor (AMF), defined by $m_{Sun} \times m_{satellite}$ where $m = \sec(\theta)$, can affect retrieval accuracy. Figure 11 shows the retrieval error dependence on the AMF. We expected the retrieval errors to decrease with the AMF because of increased sensitivity; however, the pattern is more complicated because the retrieval errors are functions of AOD, Θ, and aerosol type. For both algorithms, retrieval stability increases (decreasing standard deviation) with the AMF partially because of increasing sensitivity. However, the MB shows different behavior; it decreases in the negative regime and then increases in the positive regime with increasing AMF for AMF < 1.6, and then gradually decreases with increasing AMF. For the high AOD case, however, a high AMF does not guarantee retrieval stability; the standard deviation is uncorrelated with the AMF. For the test algorithm, the MB tends to decrease with increasing AMF except for the bifurcation observed for AMF < 1.5, while no dependency is observed for the C005 algorithm.

6   Conclusions

We quantitatively assessed the impact of the use of new aerosol models on AOD retrieval from spectral reflectance observed by Aqua-MODIS over the global ocean for the period from 2003 to 2010. AERONET inversion data and the optical property data of tri-axial ellipsoidal dust particles from an existing database were used to compile AOP in order to calculate LUTs, which include various aerosol types from absorbing to non-absorbing (0.85 < SSA < 1.00) and from fine- to coarse-dominated (0.2 or 0.3 < FMF < 1.0). Because the MODIS C005 algorithm considers only water-soluble aerosols with/without humidity for fine-mode and sea salt/dust for coarse-mode, a noticeable difference was observed in AOD retrieval using the new algorithm with the consideration of various absorptivities and the size distribution change as a function of AOD.

Validation of the algorithms by using eight years of data revealed the new aerosol models to improve the AOD, with a regression equation of y = 0.99x + 0.007 and a Pearson coefficient

of 0.93 compared to y = 0.85x + 0.028 and 0.92 for the C005 algorithm. The percentage of AOD data falling within the expected error was 64% for the test algorithm and 62% for the current operational algorithm. In particular, improvements were noted in the high AOD regime (AOD > 0.3) where the aerosol signal dominates the surface signal with a 12% increase in the number of reliable data points within the expected error. The root mean squared error (RMSE) and MB were also improved by the use of the new aerosol models.

To further characterize the retrieval errors, the data were validated with respect to AE, scattering angle, SSA, and AMF. The new aerosol models mitigated the dependence of MB (systematic error) on the aforementioned parameters. However, the coarse particle-dominated AOD was still overestimated and the fine particle-dominated AOD was underestimated. While the systematic overestimation of the coarse particle-dominated AOD increased for the high AOD case, the results for the fine particle-dominated AOD cases were similar compared to the overall case. Retrieval stability, however, was higher for the coarse particle-dominated case than the fine particle-dominated case, partially due to the wider variability in the optical properties of the fine-mode aerosols. In addition, the constrained analyses revealed the test algorithm to significantly reduce the scattering angle dependence of the retrieval error for dust-dominated cases (AE < 0.8, AOD > 0.3), partially due to improved treatment of the nonsphericity of dust particles and mitigated SSA dependence for fine-dominated cases. The standard deviation of the retrieval errors for overall case tended to decrease with AMF as expected, but no distinct tendency was observed for AOD > 0.3. Our validation results indicate that the aerosol models adopted in the current MODIS operational algorithm need to be updated to achieve better accuracy. Further analyses on FMF and SSA retrievals are required to obtain a better understanding of the various error sources contributing to AOD retrieval and corresponding improvements in the aerosol retrieval algorithms.

1 **References**

2 Bi, L., Yang, P., Kattawar, G. W., and Kahn, R.: Single-scattering properties of triaxial

3 ellipsoidal particles for a size parameter range from the Rayleigh to geometric-optics regimes,

4 Appl. Opt., 48(1), 114 – 126, 2009.

5 Bohren, C. F. and Huffman, D. R.: Absorption and scattering of light by small particles, New

6 York: Wiley-Interscience, 1983.

7 Chu, D. A., Kaufman, Y. J., Ichoku, C., Remer, L. A., Tanré, D., and Holben, B. N.:

8 Validation of MODIS aerosol optical depth retrieval over land, Geophys. Res. Lett., 29(12),

9 8007, doi:10.1029/2001GL013205, 2002.

10 Dubovik, O. and King, M. D.: A flexible inversion algorithm for retrieval of aerosol optical

11 properties from sun and sky radiance measurements, J. Geophys. Res., 105, 20,673 – 20,696,

12 2000.

13 Dubovik, O., Holben, B. N., Eck, T. F., Smirnov, A., Kaufman, Y. J., King, M. D., Tanré, D.,

14 and Slutsker, I.: Variability of absorption and optical properties of key aerosol types observed

15 in worldwide locations, J. Atmos. Sci., 59, 590 – 608, 2002.

16 Dubovik, O., Sinyuk, A., Lapyonok, T., Holben, B. N., Mishchenko, M., Yang, P., Eck, T. F.,

17 Volten, H., Muñoz, O., Veihelmann, B., van der Zande, W. J., Leon, J.–F., Sorokin, M., and

18 Slutsker, I.: Application of spheroid models to account for aerosol particle nonsphericity in

19 remote sensing of desert dust, J. Geophys. Res., 111, D11208, doi:10.1029/2005JD006619,

20 2006.

21 Hess, M., Koepke, P., and Schult, I.: Optical properties of aerosols and clouds: The software

22 package OPAC, B. Am. Meteorol. Soc., 79, 831 – 844, 1998.

23 Higurashi, A., and Nakajima, T.: Development of a two-channel aerosol retrieval algorithm

24 on a global scale using NOAA AVHRR, J. Atmos. Sci., 56, 924 – 941, 1999.

25 Higurashi, A., and Nakajima, T.: Detection of aerosol types over the East China Sea near

26 Japan from four-channel satellite data, Geophys. Res. Lett., 29(17), 1836,

27 doi:10.1029/2002GL015357, 2002.

28 Holben, B. N., Eck, T. F., Slutsker, I., Tanré, D., Buis, J. P., Setzer, A., Vermote, E., Reagan,

29 J. A., Kaufman, Y. J., Nakajima, T., Lavenu, F., Jankowiak, I., and Smirnov, A.: AERONET-

A federated instrument network and data archive for aerosol characterization, Remote Sens. Environ., 66, 1 – 16, 1998.

Hsu, N. C., Tsay, S. C., King, M. D., and Herman, J. R.: Aerosol retrievals over bright-reflecting source regions, IEEE Trans. Geosci. Remote Sens., 42(3), 557 – 569, 2004.

Hsu, N. C., Tsay, S. C., King, M. D., and Herman, J. R.: Deep blue retrievals of Asian aerosol properties during ACE-Asia, IEEE Trans. Geosci. Remote Sens., 44(11), 3180 – 3195, 2006.

Ichoku, C., Chu, D. A., Mattoo, S., Kaufman, Y. J., Remer, L. A., Tanré, D., Slutsker, I., and Holben, B. N.: A spatio-temporal approach for global validation and analysis of MODIS aerosol products, Geophys. Res. Lett., 29(12), 8006, doi:10.1029/2001GL013206, 2002.

IPCC, Climate Change 2007: The Physical Science Basis, Contribution of Working Group I to the Fourth Assessment Report of the Intergovernmental Panel on Climate Change. In: Solomon, S., Qin, D., Manning, M., Chen, Z., Marquis, M., Averyt, K. B., Tignor, M., and Miller, H. L. (Eds.), Cambridge University Press, Cambridge, United Kingdom and New York, NY, USA, 2007.

Jethva, H., Satheesh, S. K., Srinivasan, J., and Levy, R. C.: Improved retrieval of aerosol size-resolved properties from moderate resolution imaging spectroradiometer over India: Role of aerosol model and surface reflectance, J. Geophys. Res., 115, D18213, doi:10.1029/2009JD013218, 2010.

Kaufman, Y. J., Tanré, D., Remer, L. A., Vermote, E. F., Chu, A., and Holben, B. N.: Operational remote sensing of tropospheric aerosol over land from EOS moderate resolution imaging spectroradiometer, J. Geophys. Res., 102(D14), 17,051 – 17,067, 1997.

Kim, J., Lee, J., Lee, H. C., Higurashi, A., Takemura, T., and Song, C. H.: Consistency of the aerosol type classification from satellite remote sensing during the Atmospheric Brown Cloud–East Asia Regional Experiment campaign, J. Geophys. Res., 112, D22S33, doi:10.1029/2006JD008201, 2007.

Kim, J., Yoon, J. -M., Ahn, M. H., Sohn, B. J., and Lim, H. S.: Retrieving aerosol optical depth using visible and mid-IR channels from geostationary satellite MTSAT-1R, Int. J. Remote Sens., 29(21), 6181−6192, 2008.

17

Knapp, K. R., Vonder Haar, T. H., and Kaufman, Y. J.: Aerosol optical depth retrieval from GOES-8: Uncertainty study and retrieval validation over South America, J. Geophys. Res., 107, D74055, doi:10.1029/2001JD000505, 2002.

Lee, J., Kim, J., Song, C. H., Kim, S. B., Chun, Y., Sohn, B. J., and Holben, B. N.: Characteristics of aerosol types from AERONET sunphotometer measurements, Atmos. Environ., 44, 3110 – 3117, doi:10.1016/ j.atmosenv.2010.05.035, 2010a.

Lee, J., Kim, J., Song, C. H., Ryu, J. –H., Ahn, Y. –H., and Song, C. K.: Algorithm for retrieval of aerosol optical properties over the ocean from the geostationary ocean color imager, Remote Sens. Environ., 114, 1077 – 1088, doi:10.1016/j.rse.2009.12.021, 2010b.

Levy, R. C., Remer, L. A., and Dubovik, O.: Global aerosol optical properties and application to Moderate Resolution Imaging Spectroradiometer aerosol retrieval over land, J. Geophys. Res., 112, D13210, doi:10.1029/2006JD007815, 2007a.

Levy, R. C., Remer, L. A., Mattoo, S., Vermote, E. F., and Kaufman, Y. J.: Second-generation operational algorithm: Retrieval of aerosol properties over land from inversion of Moderate Resolution Imaging Spectroradiometer spectral reflectance, J. Geophys. Res., 112, D13211, doi:10.1029/2006JD007811, 2007b.

Levy, R. C., Remer, L. A., Kleidman, R. G., Mattoo, S., Ichoku, C., Kahn, R., and Eck, T. F.: Global evaluation of the Collection 5 MODIS dark-target aerosol products over land, Atmos. Chem. Phys., 10, doi:10.5194/acp-10-10399-2010, 2010.

Mayer, B., and Kylling, A.: Technical note: The libRadtran software package for radiative transfer calculations – description and examples of use, Atmos. Chem. Phys., 5, 1855 – 1877, SRef-ID: 1680-7324/acp/2005-5-1855

, 2005.

Meng, Z., Yang, P., Kattawar, G. W., Bi, L., Liou, K. N., and Laszlo, I.: Single-scattering properties of tri-axial ellipsoidal mineral dust aerosols: A database for application to radiative transfer calculations, J. Aerosol Sci., 41, 501 – 512, doi:10.1016/j.jaerosci.2010.02.008, 2010.

Mielonen, T., Arola, A., Komppula, M., Kukkonen, J., Koskinen, J., de Leeuw, G., and Lehtinen, K. E. J.: Comparison of CALIOP level 2 aerosol subtypes to aerosol types derived from AERONET inversion data, Geophys. Res. Lett., 36, L18804, doi:10.1029/2009GL039609, 2009.

Mishchenko, M. I. and Travis, L. D.: Capabilities and limitations of a current FORTRAN implementation of the T-matrix method for randomly oriented rotationally symmetric scatterers, J. Quant. Spectrosc. Radiat. Transfer, 60, 309 – 324, 1998.

Mishchenko, M. I., Geogdzhayev, I. V., Cairns, B., Rossow, W. B., and Lacis, A. A.: Aerosol retrievals over the ocean by use of channels 1 and 2 AVHRR data: Sensitivity analysis and preliminary results, Appl. Opt., 38, 7325 – 7341, 1999.

Pope, C. A., and Dockery, D. W.: Health effects of fine particulate air pollution: Lines that connect, J. Air & Waste Manage. Assoc., 56(6), 709 – 742, 2006.

Remer, L. A., Tanré, D., Kaufman, Y. J., Ichoku, C., Mattoo, S., Levy, R., Chu, D. A., Holben, B., Dubovik, O., Smirnov, A., Martins, J. V., Li, R. –R., and Ahmad, Z.: Validation of MODIS aerosol retrieval over ocean, Geophys. Res. Lett., 29(12), 8008, doi:10.1029/2001GL013204, 2002.

Remer, L. A., Kaufman, Y. J., Tanré, D., Mattoo, S., Chu, D. A., Martins, J. V., Li, R. –R., Ichoku, C., Levy, R. C., Kleidman, R. G., Eck, T. F., Vermote, E., and Holben, B. N.: The MODIS aerosol algorithm, products and validation, J. Atmos. Sci., 62, 947 – 973, 2005.

Remer, L. A., Tanré, D., and Kaufman, Y. J.: Algorithm for remote sensing of tropospheric aerosol from MODIS: Collection 5, MODIS Algorithm Theoretical Basis Document, http://modis-atmos.gsfc.nasa.gov/MOD04_L2/atbd.html.

Remer, L. A., Kleidman, R. G., Levy, R. C., Kaufman, Y. J., Tanré, D., Mattoo, S., Martins, J. V., Ichoku, C., Koren, I., Yu, H., Holben, B. N.: Global aerosol climatology from the MODIS satellite sensors, J. Geophys. Res., 113, D14S07, doi:10.1029/ 2007JD009661, 2008.

Tanré, D., Kaufman, Y. J., Herman, M., and Mattoo, S.: Remote sensing of aerosol properties over oceans using the MODIS/EOS spectral radiances, J. Geophys. Res., 102(D14), 16,971 – 16,988, 1997.

Wang, J., Christopher, S. A., Brechtel, F., Kim, J., Schmid, B., Redemann, J., Russell, P. B., Quinn, P., and Holben, B. N.: Geostationary satellite retrievals of aerosol optical thickness during ACE-Asia, J. Geophys. Res., 108, 1 – 14, 2003.

Wang, J. and Martin, S. T.: Satellite characterization of urban aerosols: Importance of including hygroscopicity and mixing state in the retrieval algorithms, J. Geophys. Res., 112, D17203. doi:10.1029/ 2006JD008078, 2007.

19

1   Yang, P. and Liou, K. N.: Geometric-optics-integral-equation method for light scattering by

2   nonspherical ice crystals, Appl. Opt., 35(33), 6568 – 6584, 1996.

3   Yang, P., Feng, Q., Hong, G., Kattawar, G. W., Wiscombe, W. J., Mishchenko, M. I.,

4   Dubovik, O., Laszlo, I., Sokolik, I. N.: Modeling of the scattering and radiative properties of

5   nonspherical dust-like aerosols, J. Aerosol Sci., 38(10), 995 – 1014, 2007.

6   Yurkin, M. A. and Hoekstra, A. G.: User Manual for the Discrete Dipole Approximation

7   Code ADDA v. 0.79, http://a-dda.googlecode.com/svn/tags/rel_0_79/doc/manual.pdf, 2009.

8

1   Table 1. LUT dimensions for the MODIS over-ocean algorithm.

Variable Name	No. of Entries	Entries
Wavelength (λ)	7	470, 555, 650, 860, 1240, 1630, 2120 nm (band 3, 4, 1, 2, 5, 6, 7, respectively)
SZA (θ_o)	8	0, 10, …, 70°
SAZA (θ_s)	8	0, 10, …, 70°
RAA (ϕ)	19	0, 10, …, 180°
AOD (τ)	9	0.0, 0.1, 0.3, 0.6, 1.0, 1.5, 2.1, 2.8, 3.6
Aerosol Model	23	Classified by FMF and SSA from AERONET inversion data

2   SZA: solar zenith angle, SAZA: satellite zenith angle, RAA: relative azimuth angle.

3

Model No. (SSA, FMF)	440 nm	675 nm	870 nm	1020 nm	1240 nm	1640 nm	2120 nm	AE	r_{eff} (μm)	sphericity
H1 (0.875, 0.25)	0.875 - 0.879 / 0.752 - 0.763	0.932 - 0.933 / 0.723 - 0.733	0.940 - 0.946 / 0.728 - 0.739	0.944 - 0.951 / 0.732 - 0.742	0.990 - 0.991 / 0.729 - 0.731	0.985 - 0.986 / 0.733 - 0.734	0.994 - 0.995 / 0.736 - 0.738	0.16 - 0.22	0.76 - 1.08	1% - 1%
H2 (0.875, 0.35)	0.877 - 0.877 / 0.719 - 0.726	0.920 - 0.922 / 0.696 - 0.698	0.929 - 0.932 / 0.705 - 0.710	0.934 - 0.938 / 0.716 - 0.720	0.989 - 0.989 / 0.725 - 0.726	0.982 - 0.983 / 0.731 - 0.732	0.993 - 0.993 / 0.735 - 0.735	0.27 - 0.28	0.61 - 0.63	2% - 3%
H3 (0.875, 0.45)	0.874 - 0.884 / 0.701 - 0.704	0.902 - 0.914 / 0.674 - 0.679	0.916 - 0.925 / 0.673 - 0.681	0.920 - 0.928 / 0.690 - 0.699	0.988 - 0.988 / 0.718 - 0.718	0.979 - 0.979 / 0.727 - 0.728	0.992 - 0.992 / 0.730 - 0.731	0.32 - 0.43	0.53 - 0.54	9% - 10%
H4 (0.875, 0.55)	0.877 - 0.880 / 0.695 - 0.702	0.883 - 0.902 / 0.664 - 0.667	0.898 - 0.913 / 0.657 - 0.661	0.905 - 0.916 / 0.674 - 0.675	0.986 - 0.986 / 0.702 - 0.709	0.974 - 0.975 / 0.715 - 0.720	0.991 - 0.991 / 0.723 - 0.725	0.43 - 0.60	0.47 - 0.50	17% - 21%
H5 (0.875, 0.65)	0.873 - 0.873 / 0.702 - 0.702	0.871 - 0.871 / 0.659 - 0.659	0.881 - 0.881 / 0.651 - 0.651	0.882 - 0.882 / 0.654 - 0.654	0.984 - 0.984 / 0.684 - 0.684	0.969 - 0.969 / 0.704 - 0.704	0.989 - 0.989 / 0.717 - 0.717	0.79 - 0.79	0.45 - 0.45	28% - 28%
H6 (0.875, 0.75)	0.875 - 0.882 / 0.706 - 0.736	0.860 - 0.873 / 0.643 - 0.659	0.855 - 0.865 / 0.627 - 0.631	0.854 - 0.857 / 0.627 - 0.634	0.981 - 0.982 / 0.617 - 0.639	0.951 - 0.955 / 0.642 - 0.665	0.982 - 0.984 / 0.675 - 0.690	1.24 - 1.28	0.34 - 0.36	67% - 74%
H7 (0.875, 0.85)	0.874 - 0.880 / 0.703 - 0.735	0.846 - 0.876 / 0.618 - 0.663	0.827 - 0.868 / 0.584 - 0.617	0.814 - 0.861 / 0.580 - 0.614	0.975 - 0.979 / 0.591 - 0.602	0.933 - 0.944 / 0.622 - 0.623	0.974 - 0.978 / 0.663 - 0.666	1.33 - 1.48	0.28 - 0.32	74% - 74%
H8 (0.875, 0.95)	0.877 - 0.881 / 0.704 - 0.713	0.850 - 0.869 / 0.601 - 0.630	0.814 - 0.858 / 0.547 - 0.575	0.787 - 0.842 / 0.523 - 0.546	0.966 - 0.969 / 0.517 - 0.536	0.891 - 0.899 / 0.526 - 0.530	0.947 - 0.949 / 0.585 - 0.594	1.65 - 1.69	0.21 - 0.23	96% - 97%
M1 (0.925, 0.25)	0.909 - 0.912 / 0.746 - 0.752	0.956 - 0.963 / 0.723 - 0.730	0.962 - 0.971 / 0.726 - 0.734	0.965 - 0.973 / 0.732 - 0.741	0.991 - 0.991 / 0.727 - 0.729	0.985 - 0.985 / 0.732 - 0.733	0.994 - 0.994 / 0.736 - 0.738	0.18 - 0.19	0.70 - 0.78	2% - 3%
M2 (0.925, 0.35)	0.912 - 0.914 / 0.718 - 0.723	0.940 - 0.950 / 0.690 - 0.703	0.950 - 0.959 / 0.694 - 0.707	0.955 - 0.961 / 0.706 - 0.715	0.989 - 0.990 / 0.724 - 0.727	0.982 - 0.984 / 0.731 - 0.734	0.993 - 0.994 / 0.734 - 0.737	0.23 - 0.36	0.62 - 0.76	2% - 6%
M3 (0.925, 0.45)	0.916 - 0.916 / 0.707 - 0.715	0.932 - 0.933 / 0.681 - 0.687	0.941 - 0.942 / 0.686 - 0.688	0.946 - 0.948 / 0.698 - 0.700	0.987 - 0.988 / 0.713 - 0.716	0.978 - 0.980 / 0.725 - 0.727	0.992 - 0.992 / 0.731 - 0.732	0.52 - 0.56	0.52 - 0.60	8% - 10%
M4 (0.925, 0.55)	0.922 - 0.923 / 0.707 - 0.712	0.929 - 0.930 / 0.670 - 0.673	0.935 - 0.936 / 0.670 - 0.672	0.940 - 0.940 / 0.683 - 0.685	0.985 - 0.985 / 0.696 - 0.697	0.974 - 0.974 / 0.714 - 0.715	0.990 - 0.990 / 0.725 - 0.726	0.74 - 0.76	0.45 - 0.47	12% - 16%
M5 (0.925, 0.65)	0.922 - 0.922 / 0.706 - 0.714	0.921 - 0.924 / 0.656 - 0.660	0.925 - 0.927 / 0.650 - 0.650	0.928 - 0.930 / 0.659 - 0.661	0.983 - 0.983 / 0.672 - 0.677	0.968 - 0.969 / 0.696 - 0.701	0.988 - 0.988 / 0.714 - 0.718	0.91 - 1.02	0.38 - 0.43	19% - 28%
M6 (0.925, 0.75)	0.923 - 0.924 / 0.702 - 0.703	0.909 - 0.924 / 0.639 - 0.641	0.905 - 0.924 / 0.622 - 0.628	0.905 - 0.925 / 0.629 - 0.633	0.980 - 0.980 / 0.639 - 0.650	0.956 - 0.960 / 0.671 - 0.678	0.984 - 0.985 / 0.699 - 0.704	1.21 - 1.28	0.34 - 0.35	28% - 40%
M7 (0.925, 0.85)	0.929 - 0.929 / 0.717 - 0.723	0.909 - 0.918 / 0.637 - 0.652	0.896 - 0.909 / 0.601 - 0.619	0.889 - 0.903 / 0.595 - 0.611	0.974 - 0.977 / 0.579 - 0.603	0.932 - 0.943 / 0.611 - 0.631	0.973 - 0.977 / 0.662 - 0.673	1.38 - 1.53	0.28 - 0.31	54% - 71%

M8	0.929 - 0.934	0.909 - 0.937	0.888 - 0.934	0.871 - 0.930	0.968 - 0.970	0.899 - 0.908	0.950 - 0.951	1.48 - 1.70	0.23 - 0.26	69% - 92%
(0.925, 0.95)	0.721 - 0.729	0.639 - 0.660	0.584 - 0.614	0.557 - 0.589	0.528 - 0.561	0.526 - 0.540	0.580 - 0.587			
N1	0.949 - 0.959	0.978 - 0.981	0.980 - 0.983	0.982 - 0.985	0.991 - 0.992	0.985 - 0.987	0.994 - 0.994	0.32 - 0.38	0.62 - 0.71	13% - 15%
(0.975, 0.35)	0.717 - 0.719	0.698 - 0.698	0.701 - 0.702	0.709 - 0.709	0.725 - 0.726	0.730 - 0.731	0.731 - 0.732			
N2	0.948 - 0.959	0.970 - 0.976	0.976 - 0.981	0.978 - 0.983	0.990 - 0.990	0.984 - 0.984	0.993 - 0.993	0.49 - 0.57	0.58 - 0.62	7% - 16%
(0.975, 0.45)	0.710 - 0.732	0.686 - 0.698	0.688 - 0.696	0.697 - 0.705	0.713 - 0.722	0.722 - 0.730	0.728 – 0.733			
N3	0.953 - 0.961	0.960 - 0.970	0.964 - 0.972	0.965 - 0.974	0.988 - 0.988	0.979 - 0.981	0.990 - 0.991	0.75 - 0.81	0.42 - 0.45	10% - 19%
(0.975, 0.55)	0.701 - 0.730	0.664 - 0.684	0.667 - 0.676	0.680 - 0.685	0.696 - 0.708	0.708 - 0.720	0.718 - 0.726			
N4	0.959 - 0.963	0.955 - 0.963	0.952 - 0.965	0.952 - 0.966	0.986 - 0.987	0.975 - 0.978	0.988 - 0.989	0.90 - 1.01	0.36 - 0.41	19% - 20%
(0.975, 0.65)	0.717 - 0.728	0.660 - 0.674	0.649 - 0.661	0.658 - 0.666	0.679 - 0.684	0.699 - 0.702	0.715 - 0.717			
N5	0.961 - 0.963	0.957 - 0.958	0.953 - 0.955	0.952 - 0.954	0.983 - 0.984	0.968 - 0.971	0.985 - 0.985	1.17 - 1.26	0.32 - 0.35	24% - 38%
(0.975, 0.75)	0.717 - 0.732	0.649 - 0.665	0.629 - 0.644	0.634 - 0.646	0.648 - 0.656	0.674 - 0.680	0.699 - 0.706			
N6	0.964 - 0.968	0.959 - 0.961	0.954 - 0.956	0.951 - 0.953	0.981 - 0.982	0.957 - 0.958	0.978 - 0.979	1.39 - 1.49	0.28 - 0.31	48% - 68%
(0.975, 0.85)	0.730 - 0.744	0.652 - 0.671	0.617 - 0.635	0.610 - 0.624	0.598 - 0.612	0.625 - 0.630	0.665 - 0.668			
N7	0.969 - 0.970	0.963 - 0.968	0.956 - 0.963	0.949 - 0.959	0.978 - 0.980	0.936 - 0.943	0.961 - 0.963	1.51 - 1.73	0.24 - 0.28	78% - 91%
(0.975, 0.95)	0.734 - 0.755	0.653 - 0.699	0.600 - 0.654	0.573 - 0.626	0.542 - 0.584	0.536 - 0.546	0.565 - 0.593			

1

2

1   Table 3. Statistics for a comparison of AOD retrieved from the MODIS C005 algorithm and

2   AERONET observations from 2003 to 2010 over the global ocean. The numbers in the

3   parentheses are for AOD (AERONET) > 0.3.

MODIS OP	2003	2004	2005	2006	2007	2008	2009	2010	Overall
R	0.91	0.93	0.92	0.87	0.94	0.92	0.92	0.94	0.92
Slope	0.78	0.87	0.82	0.77	0.9	0.9	0.88	0.87	0.85
y-intercept	0.04	0.02	0.03	0.04	0.02	0.03	0.03	0.03	0.03
Percentage within EE	66% (38%)	62% (37%)	62% (40%)	62% (40%)	58% (28%)	62% (43%)	64% (44%)	65% (54%)	62% (39%)
RMSE	0.06 (0.11)	0.07 (0.13)	0.05 (0.09)	0.05 (0.10)	0.06 (0.11)	0.06 (0.10)	0.05 (0.07)	0.05 (0.07)	0.06 (0.11)
MB	0.00 (-0.06)	0.00 (-0.05)	0.00 (-0.06)	0.00 (-0.06)	0.01 (-0.02)	0.01 (-0.01)	0.02 (-0.02)	0.01 (-0.04)	0.01 (-0.04)
N	393 (50)	451 (77)	441 (47)	346 (30)	377 (38)	336 (30)	347 (29)	264 (24)	2955 (325)

4

5

1   Table 4. Same as in Table 3 except for the test algorithm.

| This study	2003	2004	2005	2006	2007	2008	2009	2010	Overall
R	0.94	0.96	0.93	0.88	0.94	0.92	0.93	0.94	0.93
Slope	1.01	1.00	0.97	0.91	1.01	1.00	1.01	1.00	0.99
y-intercept	0.01	0.01	0.01	0.02	0.01	0.01	0.01	0.00	0.01
Percentage within EE	64% (50%)	65% (55%)	65% (48%)	62% (43%)	59% (36%)	61% (60%)	66% (51%)	67% (70%)	64% (51%)
RMSE	0.05 (0.08)	0.05 (0.08)	0.05 (0.08)	0.06 (0.10)	0.06 (0.12)	0.06 (0.10)	0.05 (0.09)	0.05 (0.07)	0.05 (0.09)
MB	0.01 (0.02)	0.01 (0.01)	0.00 (0.00)	0.00 (-0.01)	0.01 (0.05)	0.01 (0.04)	0.01 (0.02)	0.00 (0.01)	0.01 (0.02)
N	393 (50)	451 (77)	441 (47)	346 (30)	377 (38)	336 (30)	347 (29)	264 (24)	2955 (325)

2
3
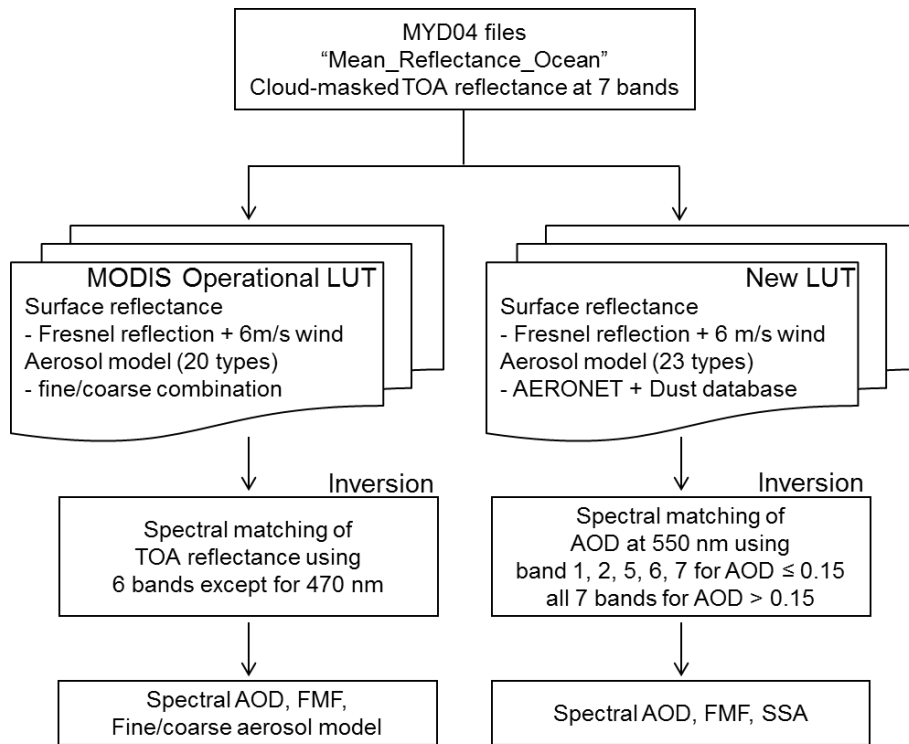
Figure 1. Schematic flowchart of aerosol retrieval by the MODIS C005 algorithm (left column) and the test algorithm (right column). The test algorithm was designed to use the same observation data ("Mean_Reflectance_Ocean" in "MYD04" files) as the C005 algorithm to evaluate the effects of the new aerosol models only. The major difference between the two algorithms is the aerosol models used to calculate the LUT.

26
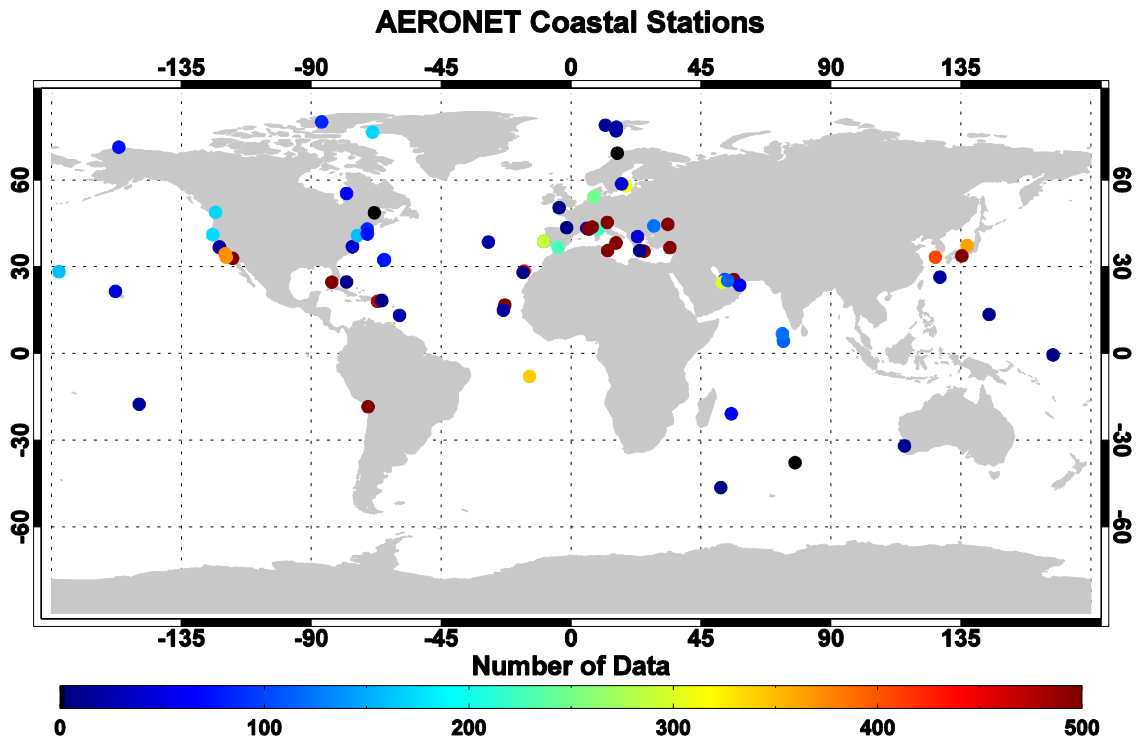
AERONET Coastal Stations

Figure 2. Global distribution of AERONET sun/sky radiometers located in coastal areas (81 stations) used to archive aerosol optical properties for the test algorithm. The colors represent the number of inversion data points at each site. AERONET stations within 7 km from the ocean were chosen as coastal stations.
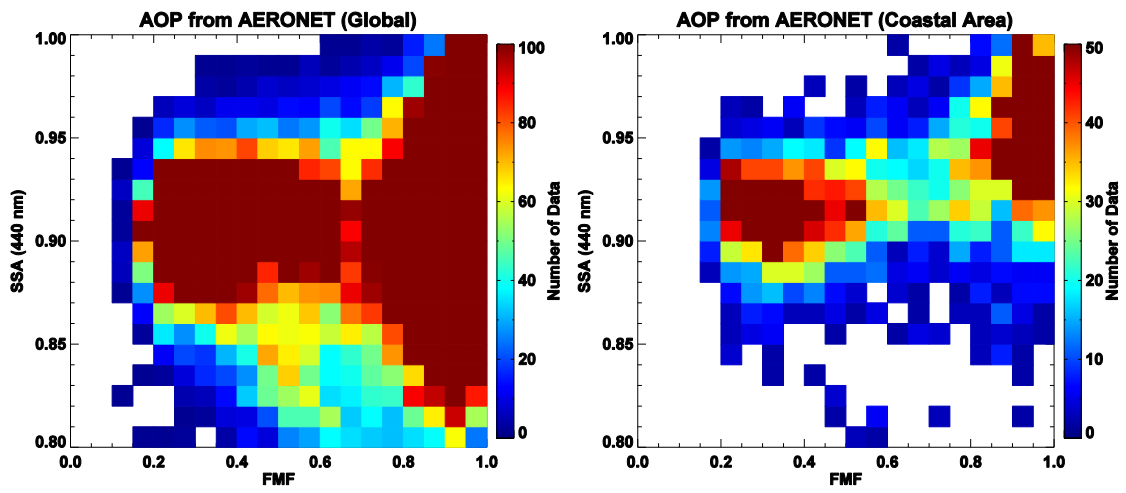
Figure 3. The number of data points included in each FMF (550 nm) and SSA (440 nm) bin, archived from the AERONET inversion data over the globe (left) and coastal areas (right). The data were sorted into intervals of 0.05 and 0.01 for FMF and SSA, respectively. The AERONET stations in the coastal area are shown in Figure 2.
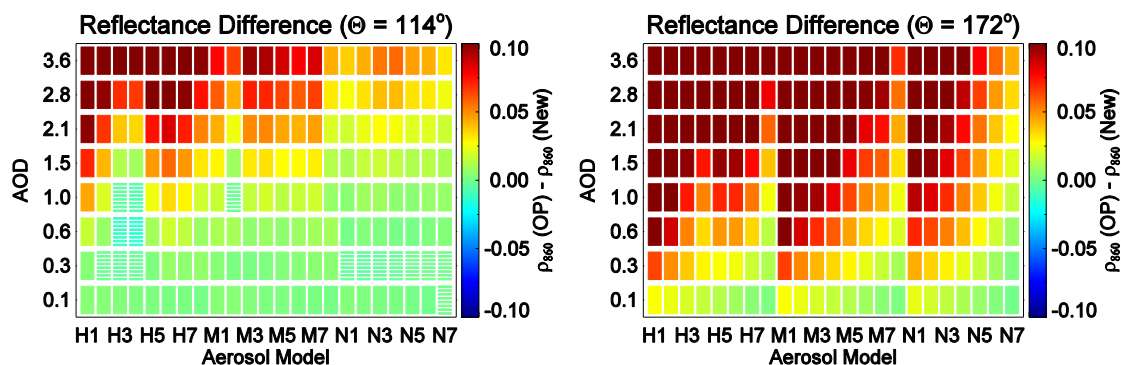
Figure 4. TOA reflectance difference at 860 nm between MODIS aerosol models and new aerosol models with respect to AOD for a given geometry. SZA (θ_o) and SAZA (θ_s) are assumed to be 50° for both tests and RAA (ϕ) is assumed to be 90° (left) and 170° (right), resulting in scattering angle (Θ) of 114° and 172°, respectively. Corresponding MODIS aerosol models to the new aerosol models are created by combining F2 ("Water Soluble") and C8 ("Dust-like type") aerosol models from Remer et al. (2006) for SSA < 0.95 and F4 ("Water Solublt with humidity") and C8 for SSA > 0.95 using FMF values from new aerosol models. Negative values are shown in line-fill.
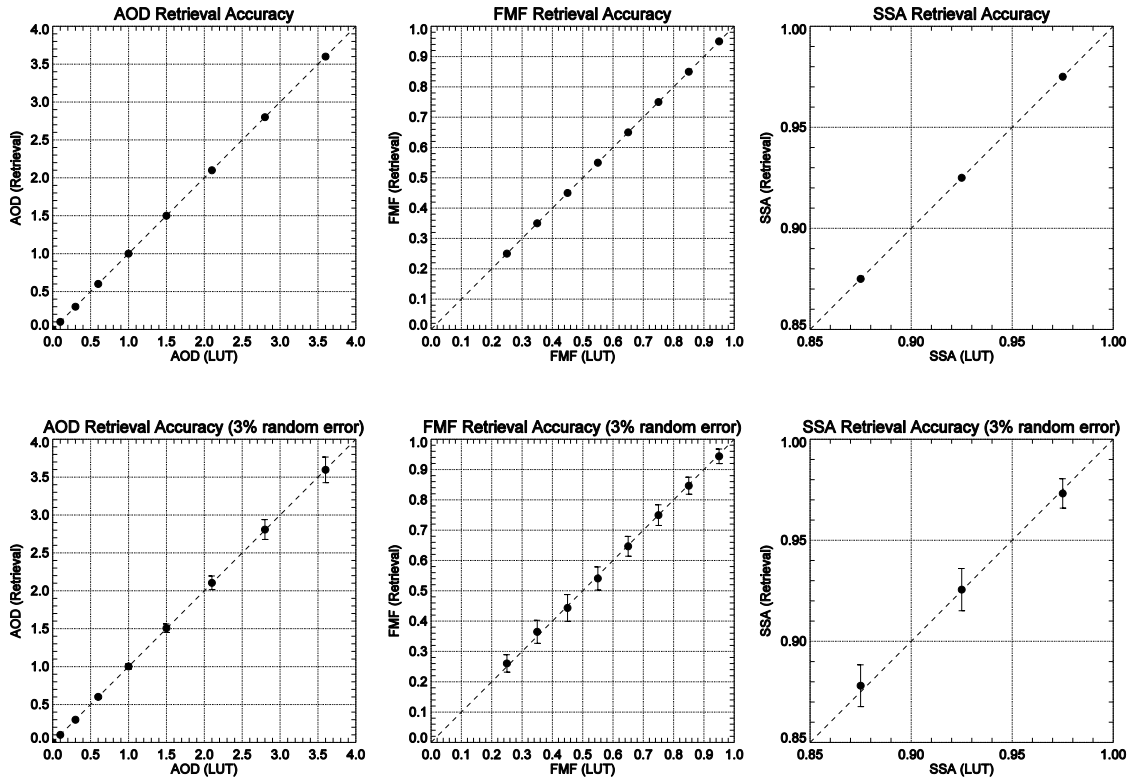
Figure 5. Comparison between input variables (AOD, FMF, SSA) and retrieved variables from the present algorithm in LUT space. Tests are performed with original data (upper) and synthesized data including maximum random error of 3% (lower). Mean and standard deviation values are shown for each calculation point for LUT.
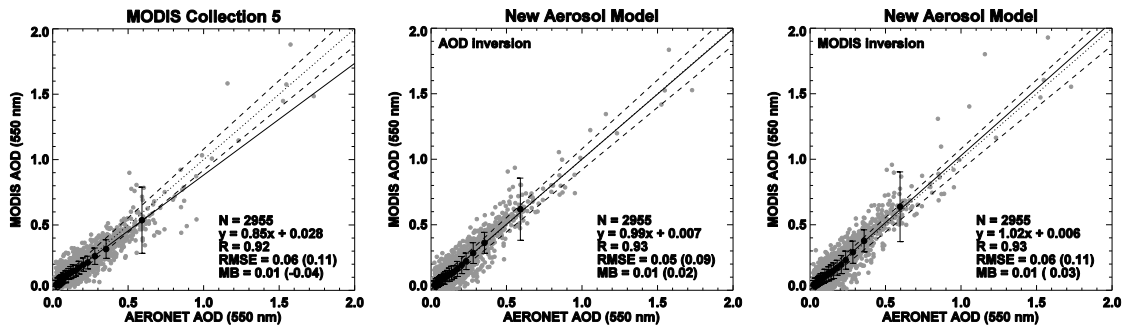
1

2

3　Figure 6. Comparison of AOD between AERONET and MODIS over the global ocean for the

4　period from 2003 to 2010. The MODIS AODs are from the C005 algorithm (left) and the test

5　algorithm (middle and right) with new aerosol models. Two different inversion procedures

6　using standard deviation of spectral AOD (middle) and MODIS operational inversion (right)

7　are applied for the test algorithm. The collocation criteria of ±30 minutes in time and 25 km in

8　space were used. The gray dots represent all data points, whereas black dots with one-

9　standard deviation interval represent mean AODs in 20 equal-number-of-data bins with

10　respect to the AERONET data. The solid line is from the regression equation, while the dotted

11　and dashed lines are the one-to-one line and the MODIS expected error (EE) line showing

12　±(0.03 + 0.05 × AOD), respectively. Only data points overlapping between the two

13　algorithms are compared. Originally, the number of data points was 3106 for the C005

14　algorithm and 3578 for the test algorithm. The statistics shown are the Pearson coefficient (R),

15　root mean squared error (RMSE), mean bias (MB), and the number of data points (N).

16

31
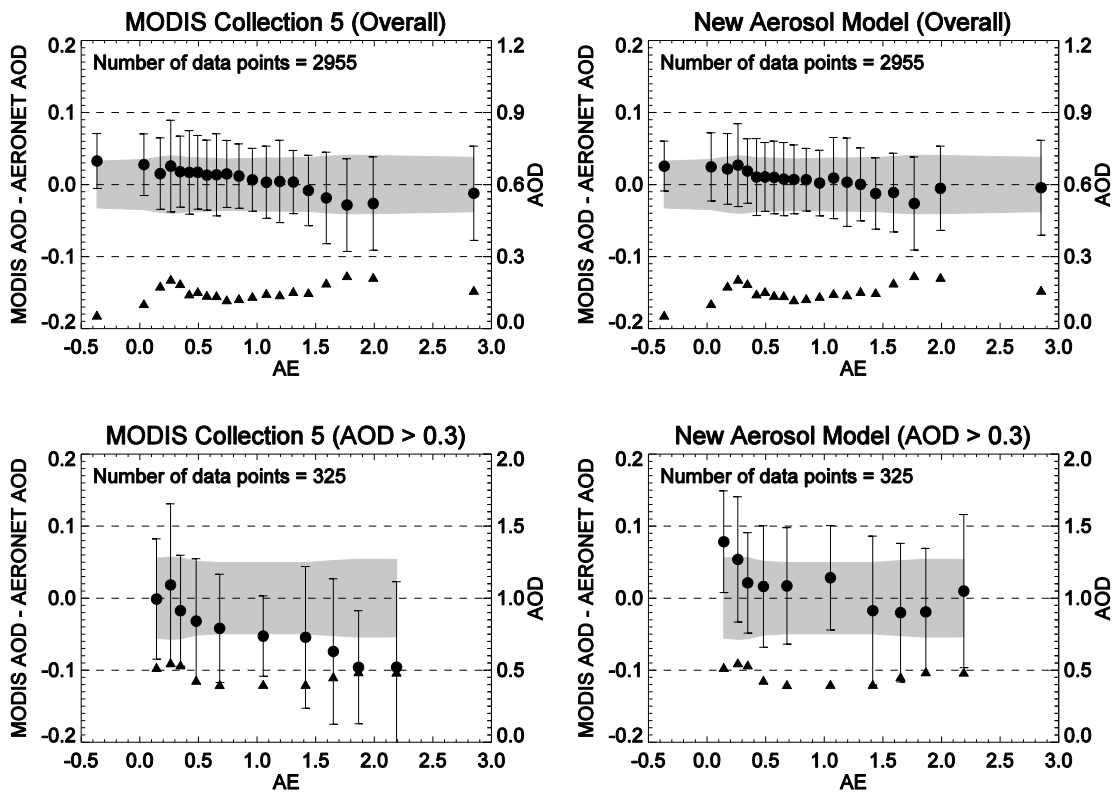
Figure 7. AE dependence of retrieval errors for the C005 algorithm (left) and the test algorithm (right) for overall data (upper) and data for AOD > 0.3 (lower). The data are sorted in 20 and 10 equal-number-of-data bins for the overall case and high AOD case, respectively. The dots and bars represent mean and one-standard deviation intervals of the retrieval errors, respectively, while the triangles represent the mean AOD from AERONET in each bin.
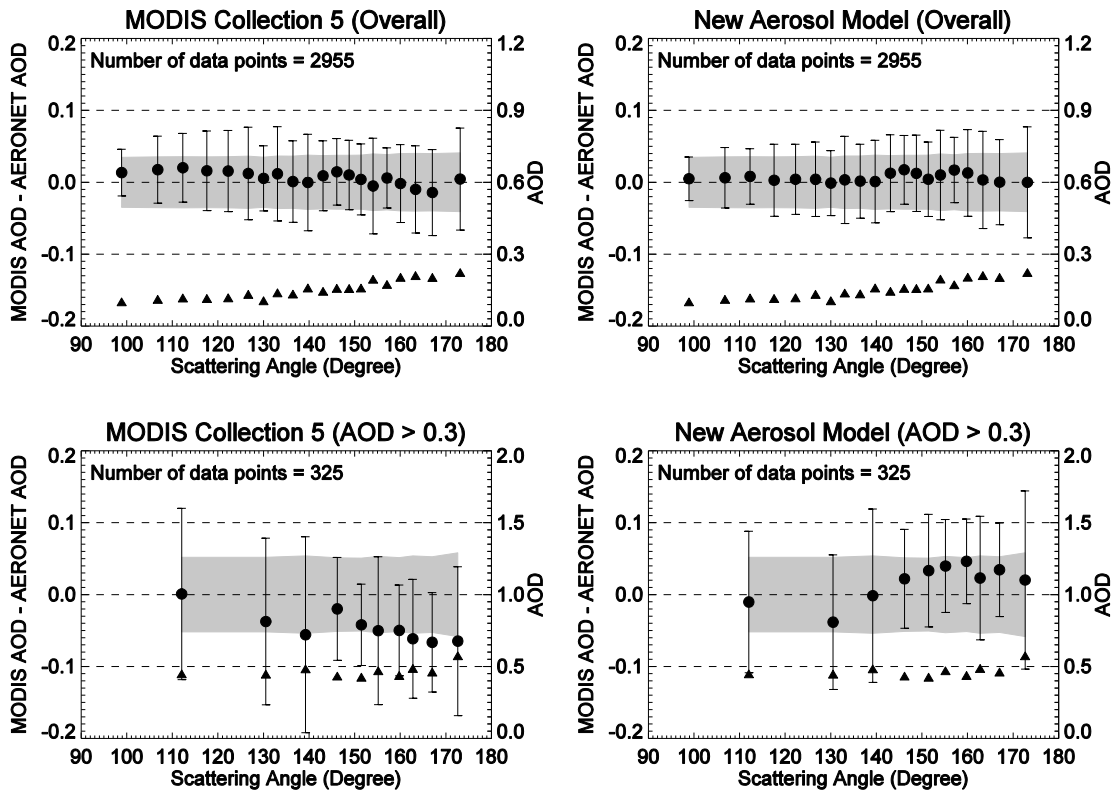
1

2

3

4 Figure 8. Scattering angle dependence of retrieval errors for the C005 algorithm (left) and the

5 test algorithm (right) for overall data (upper) and data for AOD > 0.3 (lower).

6
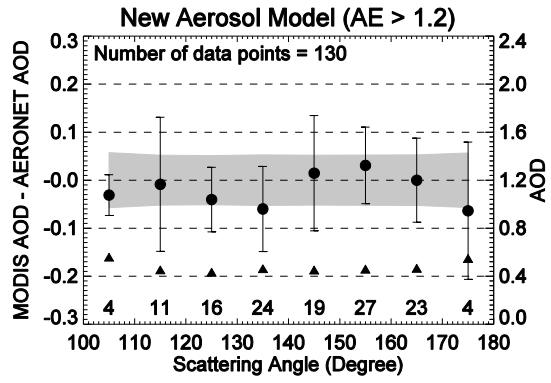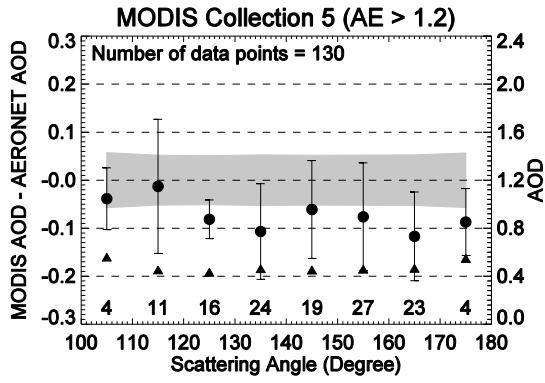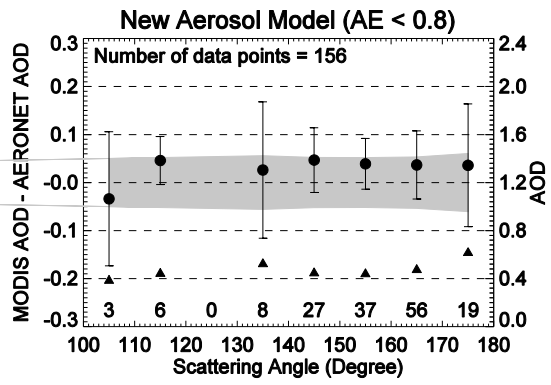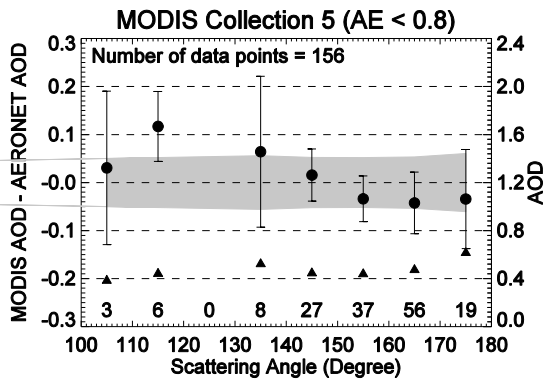
Figure 9. Scattering angle dependence of the retrieval error for C005 algorithm (left) and test algorithm (right) for AE < 0.8 (upper) and AE > 1.2 (lower). Only data with AOD > 0.3 were used in this comparison. The symbols and lines are the same as those described in the legend to Figure 7. Note that the data were sorted in each 10° interval of the scattering angle to highlight differences in the side-scattering-angle range ($100 - 130^{o}$) where the number of data points is low. The numbers on the x-axis represent the number of data points in each bin.
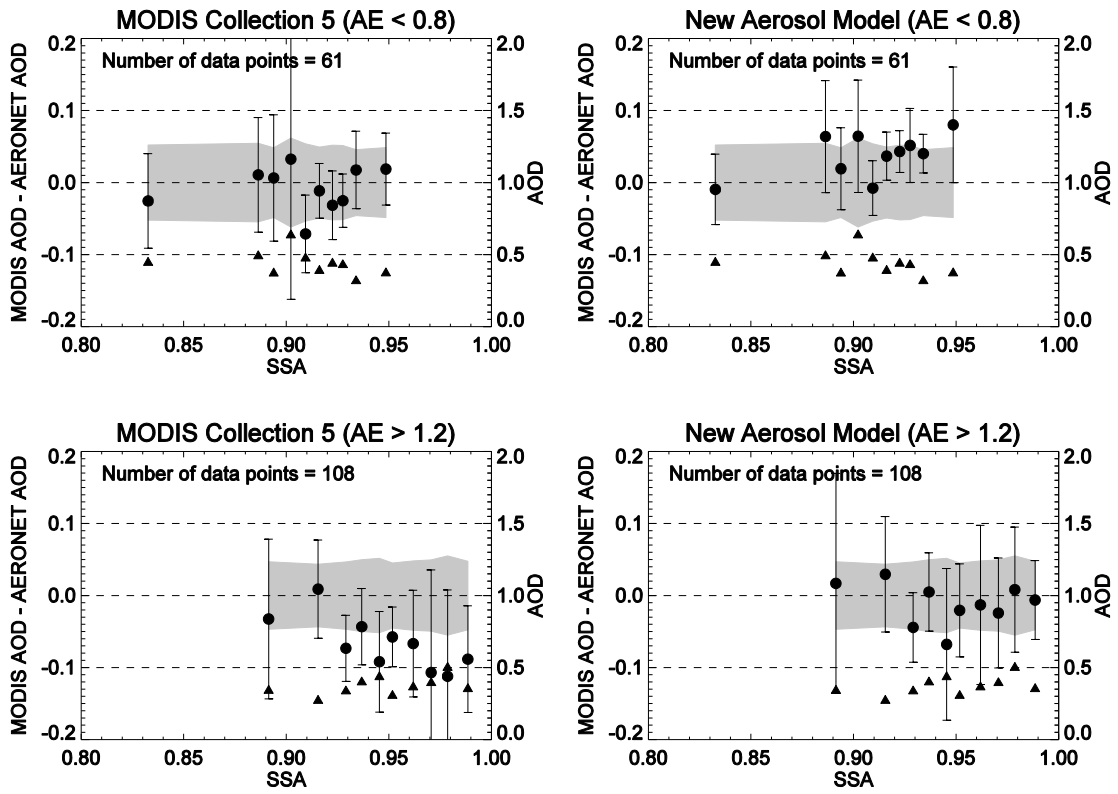
Figure 10. SSA dependence of retrieval errors for the C005 algorithm (left) and the test algorithm (right). AERONET Level 2 SSA values are retrieved for AOD (440 nm) > 0.4.
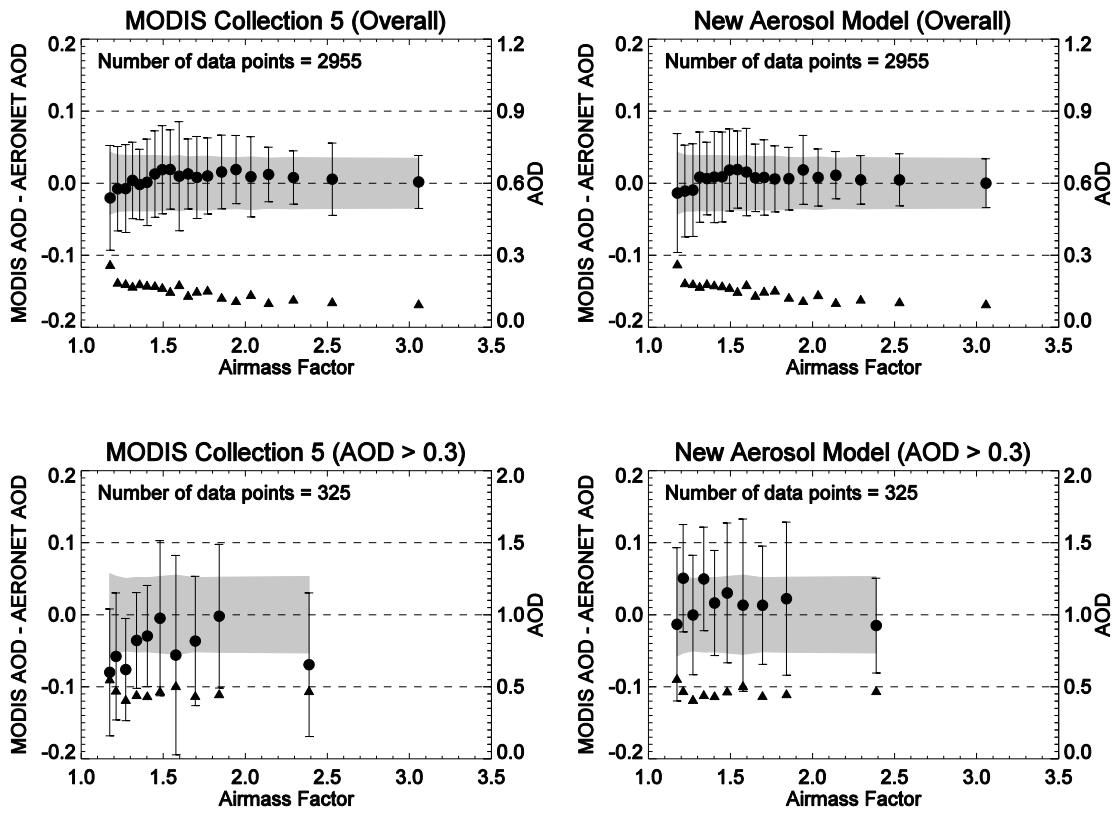
1

2

3

4　Figure 11. Air-mass factor ($m_{Sun} \times m_{satellite}$, where $m = \sec[\theta]$) dependence of retrieval errors

5　for the C005 algorithm (left) and the test algorithm (right) for overall data (upper) and data for

6　AOD > 0.3 (lower).